Comparing hexcyanoferrate loaded onto silica, silicotitanate and chabazite sorbents for Cs extraction with a continuous-flow fixed-bed setup: methods and pitfalls

Agnès Grandjean, yves Barre, Audrey Hertz, Virginie Fremy, Jeremy Mascarade, Thierry Louradour, Thierry Prevost

Comparing hexacyanoferrate loaded onto silica, silicotitanate and chabazite sorbents for Cs extraction with a continuous-flow fixed-bed setup: methods and pitfalls

Agnès Grandjean[a*], Yves Barré[a], Audrey Hertz[a], Virginie Fremy[a], Jérémy Mascarade[a], Eric Louradour[b], Thierry Prevost[c]

[a]*CEA, Univ Montpellier, DEN, DE2D, SEAD, Laboratory of Supercritical and Decontamination Processes, , F-30207 Bagnols-sur-Cèze, France*

[b]*CTI, ALSYS Group, 382 Avenue du Moulinas, 30340 Salindres, France*

[c]*Orano Cycle, Tour AREVA, 1 place Jean Millier, 92084 Paris La Défense, France*

* Corresponding author. Tel.: +33 630 146 867

E-mail address: agnes.grandjean@cea.fr (Agnès Grandjean)

A B S T R A C T

Radioactive ^{137}Cs is one of the most common and problematic radionuclides in nuclear wastes. Decontamination typically involves passing the waste in continuous flow through an agitated or fixed bed reactor containing an efficient sorbent. There are many articles in the literature describing a broad spectrum of highly efficient sorbents. However, comparing their properties is often difficult, mainly because the experimental conditions used differ. We describe the series of experiments that need to be performed to characterize Cs sorbents and illustrate by comparing three of these that, for the extraction of trace elements, the kinetics and selectivity of the exchange process are far more important than the maximum extraction capacity of the material.

Keywords: water treatment, Cs, fixed bed process, hexacyanoferrate, zeolite, silicotitanate

Non-standard abbreviations: none.

Declarations of interest: none.

1. Introduction

Most studies of solid phase extraction processes for effluent decontamination focus on the maximum sorption capacity (Q_{max}) as the main parameter to optimize [1] [2] [3]. The sorption capacity (Q) of a material is the amount or mass of contaminant captured per unit weight; the higher the sorption capacity of a material is, the less is required for a given purification or recycling process. Maximizing the sorption capacity is therefore an understandable objective. However, this maximum sorption capacity is never reached in processes for the treatment of solutions such as radioactive effluents in which the contaminants are at trace level and there are high concentrations of competitive species. In this context, comparing candidate sorbents in terms of their maximum sorption capacity at equilibrium is inappropriate.

A second important parameter for sorption materials, which is only sometimes considered [3], is their selectivity. This can be estimated by performing experiments in the presence of ions that compete for adsorption with the target species. To be relevant, these experiments have to be carried out with a ratio of competitive to target ions that is representative of actual effluents, i.e. of several order of magnitude, because the target ion (e.g. of a radioactive element) is typically at trace concentration. The distribution coefficient (K_d) is the amount of target species adsorbed relative to the amount remaining in the solution. In other words, it represents the concentration distribution of the contaminant between the solid and liquid phases. In solid phase extraction processes, the distribution coefficient is not

dimensionless and depends on experimental conditions used for a given experiment. This makes the results of different experiments difficult to compare.

The sorption capacity and distribution coefficient are measured using batch mode sorption experiments. The sorption isotherm plotted as a function of the remaining concentration of target ions (the Q-mode curve) typically plateaus at Q_{max} at high concentrations and can be fitted by a Langmuir model. The curve representing the distribution coefficient as a function of the remaining concentration of the targeted ions (the Kd-mode isotherm) is typically flat at low concentrations and then decreases linearly. The plateau value of K_d is thus the highest that can be obtained with the investigated sorbent under the experimental conditions used, with higher values being favorable for the decontamination of trace ions. For K_d estimates to be realistic and comparable however, the experiments have to be performed under representative conditions, with the same solid/solution ratio, the same kind of effluent composition (salinity, pH) and trace level contaminants.

For continuous processes, it is also important to consider the sorption kinetics and the time dependence of the sorption capacity. Here, the key parameter is the time taken to reach equilibrium. For fixed bed processes furthermore, the geometry of the setup and the initial concentration of the contaminant need to be taken into account when studying of performance of a sorbent. This is typically assessed by measuring the concentration of the target element at the outlet of a column filled with the sorbent material as a function of the volume passing through. The shape of the resulting breakthrough curve depends on the geometry of the column, the flow rate and the initial concentration of the contaminant. It has been shown that the dynamic capacity of a column is close to the maximum batch adsorption capacity, meaning that the column process is at equilibrium, provided the height/diameter ratio is greater than five [4]. For optimal performance moreover, the diameter of the column should be at least 40 times greater than the average particle diameter [5]. The flow rate is important

because fixed bed processes are only considered industrially viable at a Darcy velocity of 1 $m \cdot h^{-1}$ of higher. Finally, although this is often neglected in the literature, the shape of the breakthrough curve also depends on the contaminant concentration because decreasing it to trace levels may affect the sorption kinetics [6].

This paper compares the sorption efficiency of three ion exchangers: Sorbmatech®, a K-Cu hexacyanoferrate; a Na-Chabazite (Herschelite) type zeolite; and a Nb substituted Na crystalline silicotitanate (CST). Crystalline silicotitanates are commercially available and have been developed for a long time [7]. Their specific crystalline structure [8] with several ion exchange sites allows to be used for Cs or Sr decontamination, depending on the CST composition [9, 10]. The Nb substituted Na-CST used here has been shown to offer improved Cs sorption [11]. Zeolites are among the most widely used inorganic materials for water treatments because of their high cation exchange capacity and they have been widely studied for the removal of radionuclides [12]. While their selectivity is often low in saline solutions, they are inexpensive (naturally available) and their composition can be adjusted (Al/Si ratio, amount and nature of guest ions) to extract Cs or Sr [12]. Chabazite can accommodate various monovalent cations in its unit cell of adaptable size [13]. In a recent comparison of three zeolites with different Si/Al ratios (chabazite, stilbite and heulandite), Baek et al. [14] found that chabazite, in powder form, with the lowest Si/Al ratio, captured Cs the most rapidly with the highest sorption (exchange) capacity.

We measured sorption isotherms at two contact times (2 and 48 h) to compare the maximum sorption capacity of the three sorbents at high Cs concentration and their distribution constants at trace Cs concentration. We also measured the sorption kinetics of the three materials and performed breakthrough experiments with different Darcy velocities and inlet concentrations. This study highlights the careful experiment design and interpretation that is needed to choose a sorbent for the continuous-mode column decontamination of trace

elements from effluents. This approach is applied here for Cs removal but can be easily transposed to the removal of other trace level radioactive species such as Sr.

2. Materials and methods

2.1. Reagents

All the chemicals used in this study were supplied by Sigma Aldrich. Sea water filtered at 0.2 µm was purchased from Laboratoire Silfiac (Caen, France; composition listed in **Table 1**). The tree ion exchangers were supplied, Sorbmatech® by CTI (France), the Na-chabazite by Somez (France), and the Nb-substituted Na-CST (IE91-20) by UOP (USA). The sorption experiments were performed using seawater enriched with various concentrations of cesium nitrate or radioactive ^{137}Cs.

Table 1

Analyzed composition of sea water

Cations	**Sr2+**	**Na+**	**Mg2+**	**Ca2+**	**K+**
mg.L^{-1}	7.1	12,842	1376	444	480
Anions	Cl-	F-	Br-	SO42-	HCO3-
mg.L^{-1}	19,000	0.6	66.3	2700	142

Sorbmatech is a hierarchical granular material consisting of potassium-copper hexacyanoferrate (KCu-HCF) particles loaded onto larger silica particles that we have recently developed for the continuous selective removal of Cs [4].

CST sorbent is a Nb-substituted Na-CST ($Na_2Ti_2O_3(SiO_4),2H_2O$) and zeolite sorbent is a chabazite structure.

The powder used here consisted of chabazite grains and 20 wt% binder, water and impurities.

2.2. Characterization

X-ray diffractograms were recorded between 1.5 and 155° 2θ for 16 h using a Panalytical X'Pert MPD Pro device equipped with a Mo source ($\lambda_{K\alpha1}$ = 0.7093 Å) operated at 60 kV and 40 mA with an X'Celerator detector in Bragg-Brentano geometry. The specific surface area, pore size and pore volume of the three sorbents were obtained from nitrogen adsorption-desorption isotherms recorded at 77 K using a Micrometrics ASAP 2020 analyzer. The samples were degassed at 80 °C for 24 h beforehand.

The microstructure of the samples was observed by scanning electron microscopy (SEM) using a Carl Zeiss MERLIN device equipped with an 80 mm^2 Oxford Instruments X-MAX energy-dispersive X-ray analyzer. The samples were embedded in a non-conductive epoxy resin, polished and metallized with platinum.

The compositions of the three sorbent materials were determined by inductively coupled plasma atomic emission spectrometry (ICP-AES, Thermo Fisher Scientific iCAP 7400 DV) after dissolving them in nitric acid.

Atomic adsorption spectrometry (AAS, Perkin Elmer AAnalyst 400) was used to determine the Cs concentration in the solutions used for the sorption experiments after 10 times dilution in ultrapure (milliQ) water. The measurements were performed in triplicate for each sample with estimated uncertainties of the order of 10%. The trace concentrations of ^{137}Cs were measured by gamma spectrometry (Canberra coaxial Ge detector).

2.3. Sorption experiments

The sorption properties of the materials were first determined in batch mode from sorption isotherms and sorption kinetics. Then breakthrough column experiments were measured.

Batch sorption isotherms were measured from trace (radioactive ^{137}Cs) to high (^{133}Cs) concentrations to determine the materials' maximum sorption capacity and maximum

distribution constant. Isotherms were measured at contact times of 2 and 48 h to characterize both the initial and equilibrium sorption behavior of the materials. For the experiments with ^{133}Cs, 100 mg of the studied powder was placed in 100 mL of sea water with 2–100 mg·L^{-1} ^{133}Cs under vigorous stirring. For experiment with ^{137}Cs, 50 mg of the studied powder was placed in 50mL of sea water enriched with137Cs (35kq/L). After 2 or after 48 h (two different experiments), the supernatant was collected with a syringe, filtered through a 0.45 µm membrane and analyzed. The Cs sorption capacity (mg·g^{-1}) of the material was then calculated using Eq. 1,

$$Q_i = \left([\mathrm{Cs}]_i - [\mathrm{Cs}]_f\right)\frac{V}{m} \quad (1)$$

where $[\mathrm{Cs}]_i$ and $[\mathrm{Cs}]_f$ are the initial and final Cs concentrations, respectively, V is the volume of the solution and m the mass of solid used.

The distribution constant representing the relative proportions of the contaminant in the solid and the liquid phase was calculated from the same data using Eq. 2:

$$K_{D_i} = \frac{Q_i}{[Cs]_f} \quad (2)$$

Batch sorption kinetics were measured by placing 100 mg of the studied material in 100 mL of sea water containing either 75 mg·L^{-1} or 10 mg·L^{-1} cesium nitrate for 2–2880 min (48h) under vigorous stirring, with a separate experiment for each contact time. The supernatant was collected with a syringe at the end of each experiment and filtered through a 0.45 µm membrane before analysis.

Breakthrough curves were measured at Darcy velocities of 1 and 5 m·h^{-1} using a microcolumn (diameter, 1 cm; bed height, 3 cm) filled with the studied sorbent and solutions containing 5 or 30 mg·L^{-1} Cs (added as cesium nitrate). To make meaningful comparisons

between the three materials, the bed volume was kept constant, meaning that different masses of each sorbent were used.

3. Results and discussion

3.1. Characterization of the sorbent materials

3.1.1. Crystalline structure and chemical composition

The powder diffraction patterns obtained for Sorbmatech reveal a face centered cubic structure with Fm-3m symmetry which is characteristic of silica loaded with K-CuHCF [16, 17], and consistent with data previously reported for pure Cu-HCF powder [18]. The presence of these characteristic peaks evidences the presence of CuHCF nanoparticles. K-CuHCF consists of $Cu(NC)_6$ and $Fe(CN)_6$ octahedra linked by shared CN groups. Alkali guest ions (K+) fill the vacancies in this structure [19, 20]. Chemical analysis by ICP-AES revealed a stoichiometric excess of K (a K/Fe ratio 4), which may be due to the adsorption of KNO_3 on the silica grains. The concentration of K-CuFC particles was found to be 7 ±1 wt%. Chemical structure of CuHCF before (K as guest) and after Cs sorption (Cs as guest) was also studied using FT-IR (carried out using a Nicolet iS50) as shown on figure S1 (Supplementary Information). The v(CN) stretch was found around 2100 ± 10 cm^{-1} meaning that iron is in the (II) oxidation state [19] The v(Fe-C) stretch was recorded close to 595 cm^{-1} in good agreement for Cu-HCF (II). [21] The composition of the Nb-substituted Na-CST is 80 wt% crystalline silicotitanate (analysed formula Na/Si=1.84; Nb/Si=0.4 and Ti/Si=1.4; (Ti+Nb)/Si=2), and 20 wt% $Zr(OH)_4$ binder. It has a tetragonal structure with $P4_2/mcm$ symmetry, consisting of tetrahedral SiO_4 and octahedral TiO_6 with c-axis tunnels and vacancies at the SiO_4 sites. Guest ions (here Na^+) fill these open sites and can exchange with solution ions such as Cs or Sr. The coordination of the alkali cations can also be completed by

bonding to water molecules in the tunnels [11]. The powder diffractogram of the CST sorbent shows the typical features of a protonated CST.

Zeolites have a crystalline structure consisting of corner-sharing SiO_4 and AlO_4 tetrahedra. The Al tetrahedra are charge balanced by guest cations. Almost any alkali or alkaline earth cation can be incorporated by varying the Al/Si ratio [12]. The unit cell of chabazite consists of six-membered rings linked by tilted four-membered rings [15], with large cavities offering excellent ion-exchange properties. The chemical composition of the chabazite grains is 68.1 wt% SiO_2, 18.59 wt% Al_2O_3, 8.32 wt% Na_2O, 2.84 wt% Fe_2O_3, 1.12 wt% K_2O, 0.75 wt% MgO, and 0.27 wt% CaO. The X-ray powder pattern of the zeolite sorbent confirms that it is chabazite ($(Na, Ca, K)AlSi_2O_6.3H_2O$) with extra lines that are tentatively assigned to heulandite ($((K,Na,Ca)_2Al_3(Al,Si)_2Si_{13}O_{36} \cdot 12H_2O)$). XRD Pattern of the three samples are reported in supplementary information (Figure S2 to S4)

3.1.2. Microstructure

Fig. 1 presents the morphology of the samples at different scales as observed by SEM.

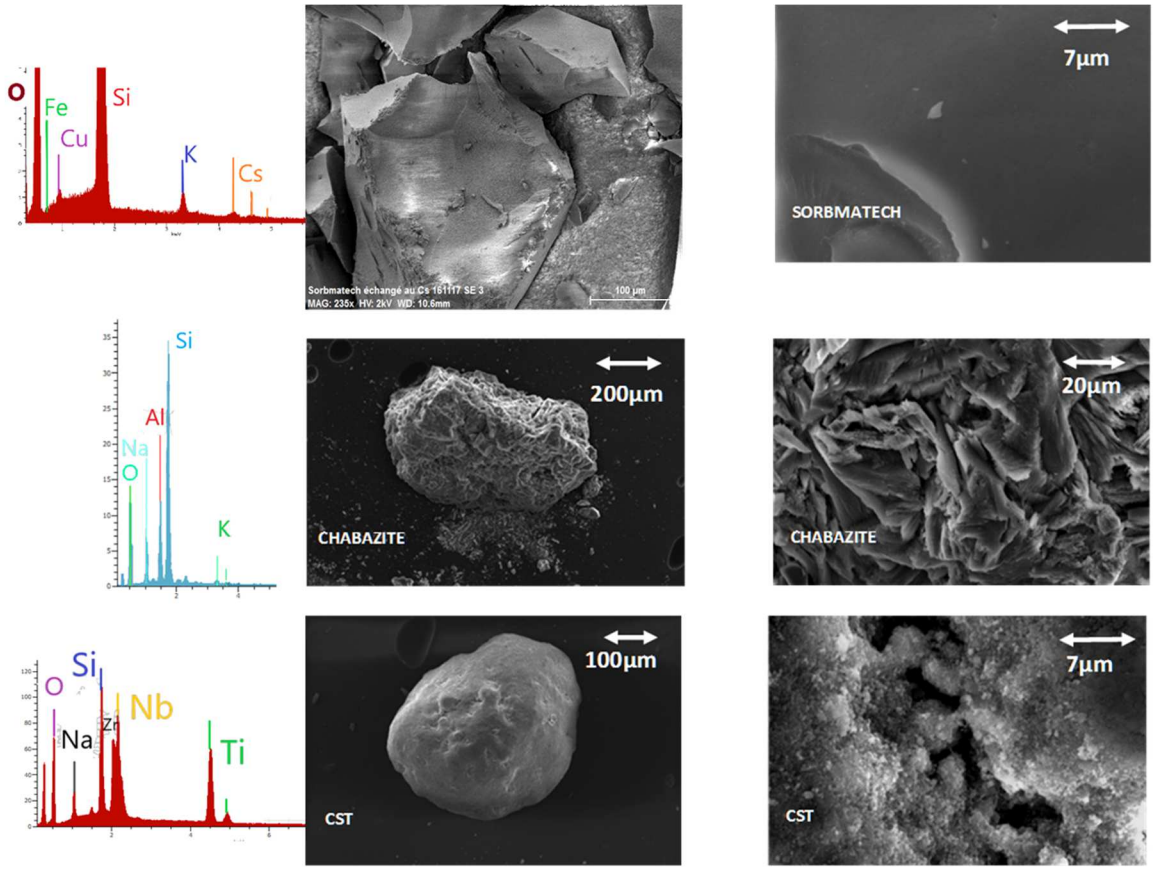

Fig. 1. Scanning electron micrographs and EDX analysis of the three sobent materisl investigated in this study: Sorbmatech (mesoporous silica functionalized with potassium-copper hexacyanoferrate nanoparticles), chabazite and a Nb-substituted Na crystalline silicotitanate (CST).

The grain sizes of all three sorbents (a few hundred µm) are compatible in-flow process using a column technology. The heterogeneities observed on the Sorbmatech particles are not K-CuHCF nanoparticles, which can only be observed by TEM [17], but are probably traces of KNO_3.

The specific surface areas and total pore volumes calculated from nitrogen adsorption experiments using the Brunauer-Emmet-Teller method are reported in Table 2.

Table 2

Porosity and ion exchange properties of the three studied sorbents

Sample	Specific surface area ($m^2 \cdot g^{-1}$)	Total pore volume ($cm^3 \cdot g^{-1}$)	Q_{max}[a] ($mg \cdot g^{-1}$)	K_d[b] ($mL \cdot g^{-1}$)
Sorbmatech	336	0.77	17.4	$2 \cdot 10^5$
Chabazite	388	0.31	> 30	94

CST	127	0.24	> 79	$7 \cdot 10^4$

CST, Nb-substituted Na crystalline silicotitanate; K_d, distribution coefficient; Q_{max}, maximum sorption capacity.

[a]Maximum sorption capacity calculated from nitrogen adsorption isotherms measured after 48 h contact time in the solution with the highest initial concentration of cesium (100 $mg \cdot g^{-1}$) for chabazite and CST, and by fitting the data using a modified Langmuir model for Sorbmatech.

[b]Distribution coefficient measured after 48 h contact time in a solution containing a trace concentration (35 $kBq \cdot L^{-1}$) of ^{137}Cs.

3.2. Batch sorption experiments

3.2.1. Maximum sorption capacity

The sorption mechanism from these sorbents is an ionic exchange between guest ions from the crystalline structure and Cs from the solution. Chemical analysis show an ionic exchange 1:1 between Cs+ from the solution and K+ from the solid in case of Sorbmatech sample, and Na+ in case of Chabazite or CST.

The sorption isotherms obtained for the three materials after 2 and 48 h are shown in **Fig. 2**. Langmuir-type behavior with a plateau at high concentrations is only observed for Sorbmatech (at both contact times) (see section isotherm modelling for the description of the fit of the data).

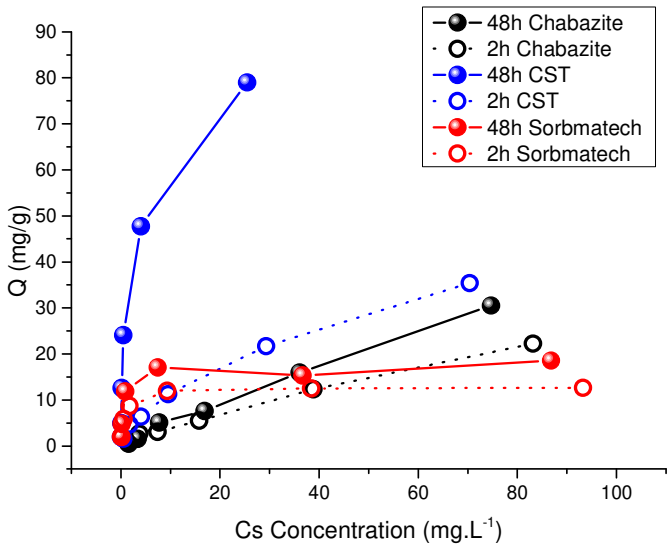

Fig. 2. Cesium sorption capacities (Q) of the three studied materials measured after 2 or 48 h in contact with seawater containing different concentrations of ^{133}Cs. Sorbmatech, mesoporous silica functionalized with potassium-copper hexacyanoferrate nanoparticles; CST, crystalline silicotitanate.

For chabazite and CST, the absence of a plateau in the isotherms indicates that the system had not reached equilibrium after 48 h. The maximum sorption capacity was taken to be the value measured in the solution with the highest initial Cs concentration (100 $mg \cdot g^{-1}$), namely 30 $mg \cdot g^{-1}$ (0.22 $mmol \cdot g^{-1}$) for chabazite and 79 $mg \cdot g^{-1}$ (0.59 $mmol \cdot g^{-1}$) for CST at 48 h, much higher than for Sorbmatech.

Fig. 2 also shows that the measured sorption capacities are lower for the shorter contact time, particularly for CST (35 vs 80 $mg \cdot g^{-1}$). For the Chabazite sample, this difference between a contact time of 2h and 48h is also very clear, with respectively a maximum of 30$mg.g^{-1}$ compared to 22$mg.g^{-1}$. In contrary, in the case of Sorbmatech, this plateau is already reached and it is close to that measured at 48h.

Previous studies indicate that the maximum sorption capacity of CSTs depend strongly on their composition and to a lesser extent on the pH of the solution. Alby et al. [3] reported maximum Cs extraction capacities of 1.9–4.4 $mmol \cdot g^{-1}$ while Clearfield et al. [11] found that Q_{max} increased slightly with the pH up to pH 6 and then plateaued to a value close to 2 $mmol \cdot g^{-1}$. The maximum Cs sorption capacity of Nb substituted Na-CST powders enriched with iron has been measured at close to 0.08 $mmol \cdot g^{-1}$ (11 $mg \cdot g^{-1}$) [10]. In their study, Miller and Brown [7] estimated measured the Cs sorption capacity of the commercial Nb-substituted CST (IONSIV IE 910) equal 2.4 $mmol \cdot g^{-1}$. All these reported experimental values are far from the theoretical maximum capacity (8 $mmol \cdot g^{-1}$) of Nb substituted Na-CST powders form available in literature [7, 10, 11, 22], or of the commercial Nb-substituted CST (IONSIV IE 910) estimated between 4 and 5 $mmol \cdot g^{-1}$ [7] This is probably because, as indicated by our data, the theoretical maximum is only approached at very long contact times. The sorption

capacities at shorter contact times are probably lower because only the surface of the material contributes.

Hexacyanoferrate materials have been widely studied for the selective removal of Cs [3]. The maximum sorption capacity measured here for Sorbmatech (0.13 mmol·g^{-1}) is much lower than the highest value reported for pure K-CuHCF powder (1.5 mmol·g^{-1}) and other loaded HCF materials [3, 23]. This is because of the relatively low HCF content of the formulation studied here. The concentration of nanoparticles estimated by taking the ratio of the maximum sorption capacities measured here and for pure HCF , ~9 wt%, is in agreement with the concentration measured by ICP-AES (6–8 wt%) .

Chabazite's order of selectivity for alkali and alkaline earth cations is Cs > K > Rb > Na = Ba > Sr > Ca > Li [13], which has been explained by a corresponding decrease in the size of the unit cell [13]. Baek et al. estimated the maximum sorption capacity of a Na-Chabazite in powder form to be 1250 mg·g^{-1} (9.4 mmol·g^{-1}) with a theoretical cation exchange capacity measured by Ba exchange of 238 mmol·g^{-1} [14]. The maximum sorption capacity measured here (0.22 mmol·g^{-1}) is much lower. This is because the chabazite powder contains 20 wt% binder and because the maximum capacity was not reached, even after 48 h (no leveling out of the isotherms in Fig. 2)[24]. The chabazite grains appear to be very dense (Fig. 1) so as for CST, the likely explanation for this behavior is that sorption only occurs on the surface of the material. A similarly low Cs sorption capacity (2–3 meq·g^{-1}) has been reported previously for chabazite in the form of composite macroporous pellets [25].

3.2.2. Distribution coefficient at trace concentration

Since Sorbmatech has a lower sorption capacity than the other two materials, the tendency in the effluent decontamination literature would be to conclude too hastily that it is less efficient. For nuclear decontamination however, the focus should be on the removal of

trace elements, which is more easily investigated using “Kd-mode” sorption isotherms measured at low contaminant concentrations, as shown in Fig. 3.

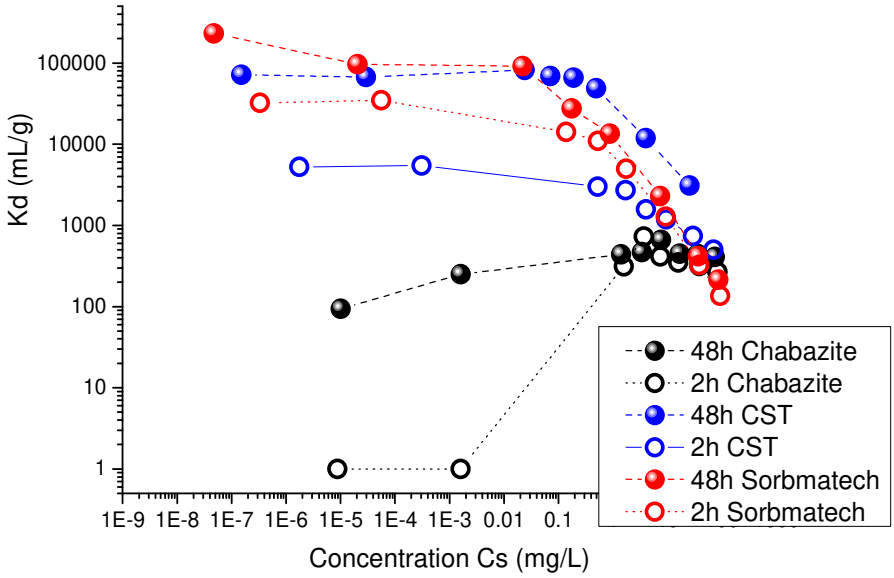

Fig. 3. Cesium distribution coefficients (K_d) in the three studied sorbent materials measured after 2 or 48 h in contact with seawater containing different concentrations of either ^{133}Cs (2-100 mg·L^{-1}) or ^{137}Cs (trace levels). Sorbmatech, mesoporous silica functionalized with potassium-copper hexacyanoferrate nanoparticles; CST, crystalline silicotitanate.

The chabazite sample, which has a relatively high maximum adsorption capacity (30 mg·g^{-1} at 48 h) is increasingly less effective than the other two materials at removing trace concentrations of Cs, with very low K_d values that tend to decrease with the Cs concentration. This is because chabazite is poorly selective for Cs in seawater. After 48 h, the distribution coefficients measured here, 1~100 mL·g^{-1}, are similar to the value measured by Baek et al. (8 mL·g^{-1}) for a chabazite powder [14]. Note that the measurements after 2 h contact carry large analytical uncertainties.

The distribution coefficients measured for CST after 2 and 48 h in low Cs solutions differ by more than an order of magnitude (Fig. 3). This is again because the CST grains are dense with very few pores, delaying the saturation of the interior. The values and trend for

Sorbmatech are similar, but the distribution coefficients for Sorbmatech are higher (lower) than those measured for CST at lower (higher) Cs concentrations. The better performance of Sorbmatech at low Cs concentrations is particularly marked initially (2 h contact time, Fig. 3). In summary, these results show that Sorbmatech or CST, with distribution constants of close to 10^5 mL·g^{-1}, are significantly more effective than chabazite for the decontamination of seawater with trace levels of Cs. Note that the results may be different for solutions other than seawater with lower concentrations of competitive cations.

Comparing distribution coefficients between studies is difficult because they depend on the Cs concentration and the nature of the solution used. As an indication nevertheless, the values measured here are in the middle of the range (~10^4 to 10^6 mL·g^{-1}) reported in the literature for measurements at trace concentrations of ^{137}Cs (a few kBq·L^{-1}) in aqueous saline solution for various HCFs [26], HCF-functionalized silica [17] and CST materials [9, 27].

3.2.3. Isotherm modelling

As mentioned above (section 3.2.1), Langmuir-type behavior with a plateau at high concentrations is only observed for Sorbmatech (at both contact times). The sorption isotherms measured at high Cs concentration for Sorbmatech are well fit with a Langmuir model [24] (Eq. 3, with L the Langmuir parameter and $[C]_{eq}$ the equilibrium concentration and Q_{max} 16 mg·g^{-1} (0.12 mmol·g^{-1})). Fig. 4 shows however that the data over the entire concentration range are only accurately fitted by the modified Langmuir model described by Eq. 4, with Q_{max}= 17.4 mg·L^{-1} and c the Langmuir modified parameter equal to 0.1.

$$Q = Q_{max}\frac{L[C]_{eq}}{1+L[C]_{eq}} \quad (3)$$

$$Q = Q_{max}\frac{L([C]_{eq})^{1-c}}{1+L([C]_{eq})^{1-c}} \quad (4)$$

Indeed, in case of decontamination of radioactive effluent, we need to fit the low concentration domain (done with ^{137}Cs at trace concentration) with accuracy. This modified model will be used for comparison to dynamic capacity for in-flow experiments.

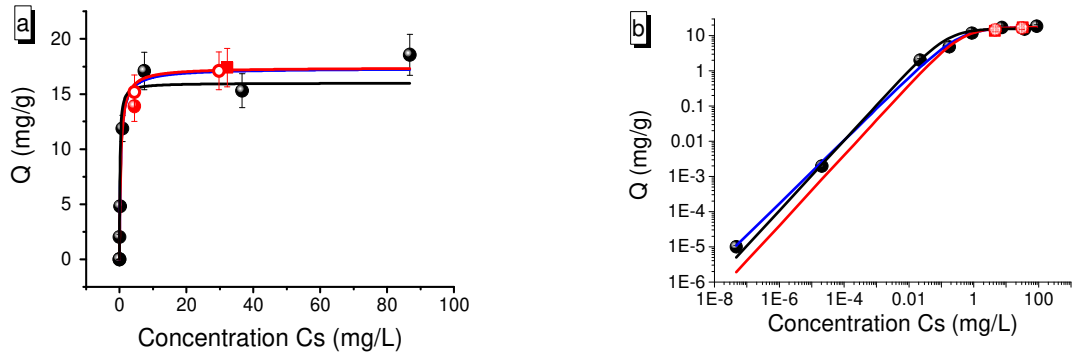

Fig. 4. Cesium sorption capacities of Sorbmatech (mesoporous silica functionalized with potassium-copper hexacyanoferrate nanoparticles) measured after 48 h in contact with seawater containing different concentrations of either ^{133}Cs (initial 2–100 mg·L^{-1}) or ^{137}Cs (trace levels) on (a) linear and (b) log-log scales. The blue and red lines are the best fits with the Langmuir and the modified Langmuir equation (Eqs. 3 and 4 in the main text), respectively. The red squares and red circles are the dynamic capacities calculated from breakthrough experiments performed at Darcy velocities of respectively 1 and 5 m·h^{-1}.

3.3. Kinetics experiments

Fig. 5 shows how the sorption capacities of the three materials increase over time.

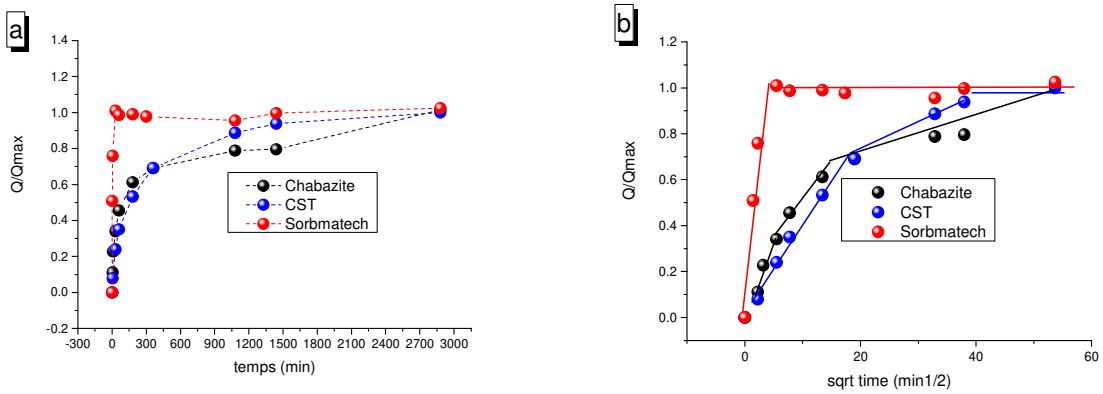

Fig. 5. Normalized cesium sorption capacities of the three studied materials as a function of (a) linear and (b) square root time as measured from batch experiments in seawater containing 70 mg·L^{-1} Cs. Sorbmatech, mesoporous silica functionalized with potassium-copper hexacyanoferrate nanoparticles; CST, crystalline silicotitanate.

It is clear that the sorption kinetics are much faster for Sorbmatech than for CST or chabazite. All three are heterogenous grains. The chabazite and CST samples contain both crystals and binder, with possible macropores between the two. The Sorbmatech grains consist of mesoporous silica particles loaded with HCF nanoparticles. Ion exchange kinetics in heterogeneous particles are governed by at least three distinct diffusional steps [25] : 1) diffusion in the boundary layer between the solution and the surface of the material; 2) diffusion through the macropores and mesopores of the grains; 3) diffusion within the microporous crystals where ion exchange takes place (here, the CST, chabazite or HCF crystals). Fig. 5b reveals the presence of several rate-limiting diffusional steps for CST and Chabazite but just one for Sorbmatech. The only limiting step for Sorbmatech is diffusion in the boundary layer (Nernst layer) around the grains. The diffusion inside the grains is not rate-limiting because the material contains mesopores and because the ionic exchanger KCu-HCF is nanosize particles [17]. The two other materials are much denser, hindering diffusion, and contain relatively large sorbent particles mixed with binder, slowing the ion exchange process. This interpretation is in keeping with Depaoli and Perona, who showed that the ion exchange rate in macroporous chabazite pellets depended both on intraparticle and external diffusion rates.[28]

Fig. 6 compares the sorption kinetics of CST and Sorbmatech in solutions with initial concentrations of 70 and 10 $mg \cdot L^{-1}$. For Sorbmatech, the initial sorption rate is slightly lower at the lower Cs concentration, which is consistent with the rate-limiting step being external mass transfer resistance through the liquid film on the surface of the grains and of the mesopores. Mass transfer is driven by the concentration gradient between the surface containing the HCF nanoparticles and the pore or bulk solution. This driving force thus decreases with the Cs concentration of the solution, and this decrease may explain the slight slowing down of the sorption process evidenced in Fig. 6.

For CST in contrast, the sorption rate is substantially higher at the lower Cs concentration, as has been observed previously by Mahendra et al. for a dense ionic exchange resin [6]. This may be because there are two ion exchange sites in CST, tunnels and framework vacancies [11], with potentially different exchange kinetics and capacities. The fast sorption at low Cs concentrations would then reflect exchange at the first site with fast kinetics and a low capacity, while the slower sorption at higher Cs concentrations is the result of sorption on the second site with a larger capacity but slower kinetics.

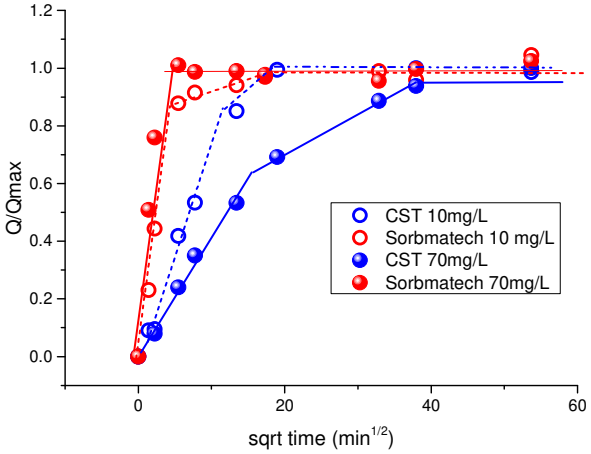

Fig. 6. Comparison of the (square-root) time-variation of the normalized cesium sorption capacities of Sorbmatech (mesoporous silica functionalized with potassium-copper hexacyanoferrate nanoparticles) and CST (a crystalline silicotitanate) in seawater containing 10 or 70 mg·L^{-1} Cs.

3.4. Continuous flow experiments

Fig. 7 shows the breakthrough curves obtained for the three sorbents with a Darcy velocity of 1 m·h^{-1} and an inlet Cs concentration of 30 mg·L^{-1}. The shape of a breakthrough curve depends on the parameters of the experiment and the material but ideally, the outlet concentration jumps instantaneously from zero to the feed concentration when the column capacity is reached.

Breakthrough curves can be divided into three main zones [29].

The first corresponds to the period during which the concentration of the studied element (Cs here) in the solution passing through the outlet is zero. The breakthrough volume (V_B) is defined by convention as corresponding to an outlet concentration equal to 1% of the input concentration. This is the volume of the studied solution that can pass through the column without any "leakage" of the species of interest and is thus the most important parameter for the decontamination of trace elements. It depends both on the physical properties of the sorbent (surface area, particle size, pore size, pore volume..) and on the parameters of the process (flow rate, temperature, bed size…) [30].

The second part of the breakthrough curve is the mass transfer region during which the outlet concentration increases sharply. In most cases, breakthrough curves are symmetric (sigmoidal) and the half-breakthrough volume or retention volume (V_R) is defined as the percolated volume at which the concentration at the outlet of the column is equal to half the concentration at the inlet. The more efficient the sorption process is, the sharper the increase in the breakthrough curve is and the closer V_R is to V_B [6].

The finally part of the breakthrough curve is the saturation phase. The saturation or hold-up volume (V_M) is defined as the outflow volume at which the outlet concentration reaches 99% of the inlet concentration. This is the minimum volume of solution needed to saturate the sorbent. The bed capacity or dynamic capacity (Q_{dyn}) at saturation is calculated from the saturation volume as follows:

$$\boldsymbol{Q_{dyn}} = \frac{\boldsymbol{V_M}[\boldsymbol{Cs}]_{\boldsymbol{inlet}} - \int_0^{\boldsymbol{V_M}} [\boldsymbol{Cs}]_{\boldsymbol{outlet}} \boldsymbol{dV}}{\boldsymbol{m}} \quad (5)$$

The dynamic capacity can be compared to the batch capacity calculated using a Langmuir model by replacing $[Cs]_{eq}$ with $[Cs]_{inlet}$ in Eq. 3 or Eq. 4. This comparison reveals whether the column process reaches equilibrium with the investigated sorbent.

Finally, another useful parameter to evaluate sorbents for the removal of trace-level contaminants is the bed efficiency (BE) [16, 31] , the proportion of the total amount of Cs that has been injected into the column at mi-breakthrough that is retained by the sorbent:

$$\mathrm{BE} = \frac{V_R * [Cs]_{inlet} - \int_{V=0}^{V_R} [Cs]_{outlet}\, dV}{V_R * [Cs]_{inlet}} \quad (6)$$

For column experiments, two parameters were studied: initial concentration ($[Cs]_{inlet}$ equal to 5mg.L^{-1} or 30mg.L^{-1}) and Darcy Velocity (1m.h^{-1} and 5m.h^{-1}). **Table 3** lists these parameters for all the breakthrough experiments performed here

Table 3

Results of breakthrough experiments performed with the three studied sorbents

Sample	Bed weight (g)	$[Cs]_{inlet}$ ($mg \cdot L^{-1}$)	Darcy velocity ($m \cdot h^{-1}$)	Bed height (cm)	V_B (mL)	V_R (mL)	Q_{dyn} ($mg \cdot g^{-1}$)	Q_{batch} ($mg \cdot g^{-1}$)	Bed efficiency (%)
Sorbmatech	1.525	4.16	1	3	2432	3268	13.5	15.5	96
	1.496	4.47	5	3	1082	3386	15.2	15.6	92
	1.314	29.74	1	3	426	563	17.1	17.0	97
	1.408	32.2	5	3	292	545	17.4	17.1	92
CST	2.144	5.68	1	3	2500	–	–	–	–
	2.240	5.16	5	3	0	4300	–	–	71
	2.113	29.28	1	3	700	–	–	–	
	2.113	29.98	1	3	300	–	–	–	
	2.135	26.9	5	3	0	1100	N/A	N/A	77
Chabazite	1.3960	30.7	1	3		450		N/A	70

Q_{batch}, maximum sorption capacity measured in batch experiments; Q_{dyn}, maximum sorption capacity measured in continuous flow experiments; V_B, breakthrough volume; V_R, retention volume.

3.4.1. Comparison of the three sorbents

Fig. 7 shows that at a Darcy velocity of 1 $m \cdot h^{-1}$ and an inlet Cs concentration of 30 $mg \cdot L^{-1}$, the breakthrough volume for chabazite is very low (~30 mL) and the breakthrough curve is flat. This early leakage can be explained by chabazite's slow sorption kinetics and poor selectivity. Sorbmatech and chabazite have similar retention volumes, respectively 563 mL and 450 mL under these conditions, but Sorbmatech has a higher bed efficiency (97% vs 70%) as highlighted by its sharper breakthrough curve. A similar column test performed by DePaoli et al. with chabazite and a solution containing ^{90}Sr and ^{137}Cs showed that the strontium was not retained in the column and was continuously replaced on chabazite by competitive cations [5]. Despite chabazite's large maximum sorption capacity for Cs (close to 30 $mg \cdot g^{-1}$), these continuous flow results show that other faster and more selective sorbents should be preferred to treat Cs contaminated seawater.

The breakthrough curve for CST is so flat that the mid-breakthrough volume was not reached even after 2 L of the Cs-enriched solution had percolated through the column. This experiment was repeated to confirm the reproducibility of the results. The two breakthrough volumes obtained were 300 and 700 mL, the large difference being due to the large uncertainties associated with the measurements of very low Cs concentrations and the heterogeneity of the CST grains (i.e. the beds in the two experiments were not identical). These values are in the same range as the breakthrough volume measured for Sorbmatech under the same conditions. Note for CST that DePaoli et al. recorded a similarly flat breakthrough curve for a different CST (Ionsiv® IE911) investigated for Sr removal [5].

Sorbmatech's breakthrough curve is close to ideal and can be fitted by a Boltzmann sigmoid function [32],

$$[Cs]_{outlet} = \frac{[Cs]_{inlet}}{1+exp\left(\frac{V-V_r}{\Delta V}\right)} \quad (7)$$

with V_R and ΔV (a volume parameter that accounts for deviation from an ideal breakthrough curve) as free parameters. The linearization of this equation corresponds to the Thomas Yoon-Nelson models [33] as:

$$ln\left(\frac{[Cs]_{outlet}}{[Cs]_{outlet}-[Cs]_{inlet}}\right) = k_{yN}t - k_{yN}\tau \quad (8)$$

Where t (h), the time is equal QV (with Q(L/h) the flow rate); τ is the half breakthrough time and k_{YN} (1/h) the Yoon Nelson parameter is equal to Q/ΔV.

The fitted value of V_R was then used to obtain a more accurate estimate of the breakthrough volume, using Eq. 8:

$$V_B = V_R + \Delta V ln\left(\frac{100}{99} - 1\right) \quad (9)$$

and of the bed efficiency, using Eq. 6, yielding V_B = 426 mL and BE = 97%. The log/log representation of the breakthrough curves in Fig. 7b highlights the differences between the breakthrough volumes and breakthrough behavior of the three sorbents. While the Yoon–Nelson model can well fitted (R2 > 0.9) with the data obtained on Sorbmatech breakthrough this is not the case for the other two sorbents.

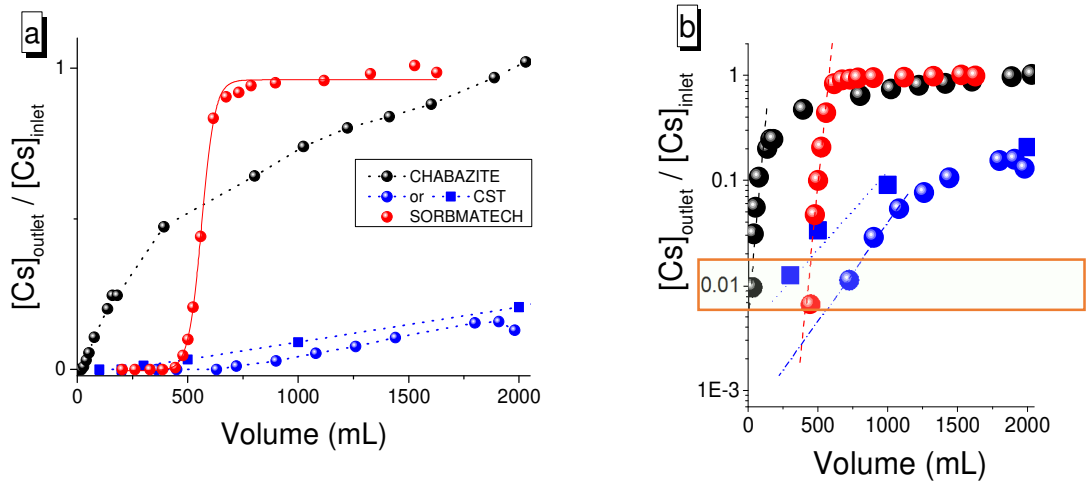

Fig. 7. Breakthrough curves ($[Cs]_{outlet}/[Cs]_{inlet}$ vs. ejected volume) for the three sorbents at a Darcy velocity of 1 $m \cdot h^{-1}$ and an inlet Cs concentration of 30 $mg \cdot L^{-1}$ shown with (a) linear and (b) logarithmic axes. The box in part b highlights the breakthrough volumes of the three sorbents, defined as the ejected volume at $[Cs]_{outlet}/[Cs]_{inlet}$ = 0.01. Sorbmatech, mesoporous silica functionalized with potassium-copper hexacyanoferrate nanoparticles; CST, Nb-substituted Na crystalline silicotitanate. Line in case of Sorbmatech corresponds to the fit of experimental data using equation 7 (Yoon–Nelson model).

These data clearly show that mass transfer between the solution and the sorbent is the key parameter governing the efficiency of the column process. It has recently been shown that the ion exchange or catalytic properties of these materials can be optimized by rigorously controlling the porous profile of the monoliths to increase the contact time with the reactant/contaminant [34-36]. The different shapes of these breakthrough curves can therefore be attributed first to differences in the microscopic structure of the sorbent grains, which affect the sorption kinetics, and second, to differences in the intrinsic selectivity of the materials, which affect the thermodynamic equilibrium.

In light of the poor performance of chabazite, the effects of different inlet concentrations and flow rates were only investigated for CST and Sorbmatech.

3.4.2. Effect of the Darcy velocity and inlet concentration

Fig. 8 compares the breakthrough curves measured for Sorbmatech at two different Darcy velocities and inlet Cs concentrations. The curves are all close to ideal, allowing them to be fitted by a sigmoidal curve (using Eq. 7) or Yoon–Nelson model and aligned by normalizing the ejected volume to the values of V_R obtained.

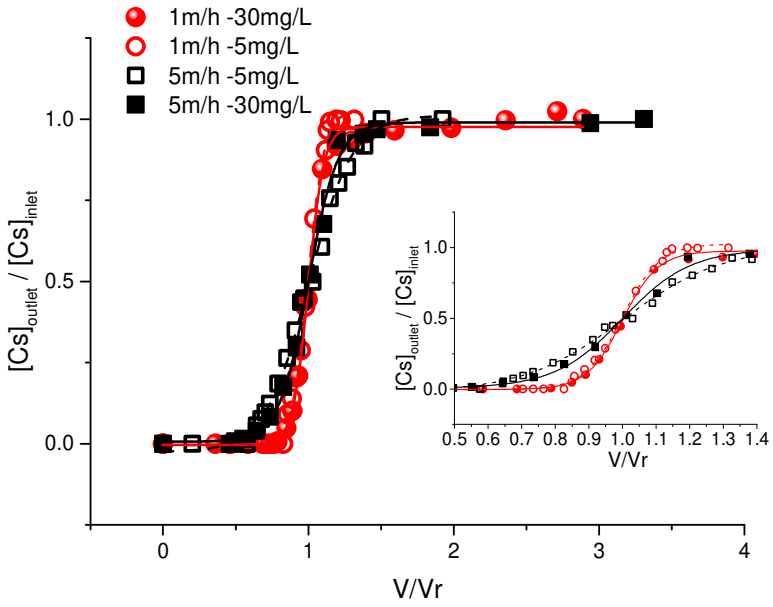

Fig. 8. Comparison of the breakthrough curves (($[Cs]_{outlet}/[Cs]_{inlet}$ vs. ejected/retention volume) measured for Sorbmatech (mesoporous silica functionalized with potassium-copper hexacyanoferrate nanoparticles) at Darcy velocities of 1 and 5 $m \cdot h^{-1}$ and inlet Cs concentrations of 5 and 30 $mg \cdot L^{-1}$. The retention volume, V_R, was calculated by fitting the experimental data using Eq. 7.

Fig. 8 shows that increasing the initial concentration at the same flow rate makes the slope of the breakthrough curve slightly sharper. This is likely because increasing the concentration and therefore the concentration gradient between the solution and the sorbent promotes external mass transfer [6]. This behavior is also consistent with the kinetics experiments, which showed a slightly lower initial sorption rate at the lower Cs concentration, and a previous study of a macroporous zeolite monolith used to remove trace concentrations of ^{90}Sr, where the breakthrough curve was sharper at the higher inlet concentration [37].

Fig. 8 also shows that increasing the flow rate (Darcy velocity) smoothens the breakthrough curves, as observed previously again for Sr adsorption using a monolithic zeolite [37]. The breakthrough (V_B) and retention (V_R) volumes are substantially lower at the higher flow rate. The bed efficiency seems to depend only on the Darcy velocity, with a BE close to 96% at 1 $m \cdot h^{-1}$ and close to 92% at 5 $m \cdot h^{-1}$ for both Cs concentrations considered. At

saturation, the dynamic capacities are all similar to the batch capacity obtained by fitting the sorption isotherm using the modified Langmuir model (Eq. 4), meaning that equilibrium was reached in all these column experiments.

The breakthrough curves obtained for CST are compared with the Sorbmatech data in Fig. 9. The curves for CST are all flat and cannot be fitted using the Yoon–Nelson model (or by a sigmoidal function). Half-breakthrough was not reached at the lower Darcy velocity (1 $m \cdot h^{-1}$), even after several liters of solution (2 L at a Cs inlet concentration of 30 $mg \cdot L^{-1}$ and 5 L at 5 $mg \cdot L^{-1}$) had percolated, making it impossible to determine V_R or BE. The breakthrough volumes of the two materials are similar at the lower Darcy velocity but at 5 $m \cdot h^{-1}$, Fig. 9 shows that the CST bed starts to leak Cs immediately, giving $V_B = 0$. The bed efficiencies of CST at this higher flow rate are roughly 71% at the lower Cs concentration and 77% at the higher one. These values were obtained directly from the curves rather than from fits so the seeming decrease of the bed efficiency with the inlet concentration is probably not significant. At the lower concentration and higher Darcy velocity, the breakthrough curve (the open blue circles in Fig. 9b) seems to consist of two linear steps, a first relatively fast increase followed by a slower one. This would be consistent with the batch sorption experiments that show faster kinetics at lower concentrations, and with our interpretation that this is due to the presence of at least two sorption sites with different sorption kinetics. Two-step breakthrough curves at high flow rates have been described previously for Sr sorption by a monolithic zeolite [38] and for Mn adsorption by granular carbon columns. In the latter study, two flow rates were investigated and the two-step behavior was only observed for the faster one[39]. Our interpretation is follows DePaoli et al., who also attributed atypical breakthrough curve with multiple steps to the presence of multiple exchange sites [5].

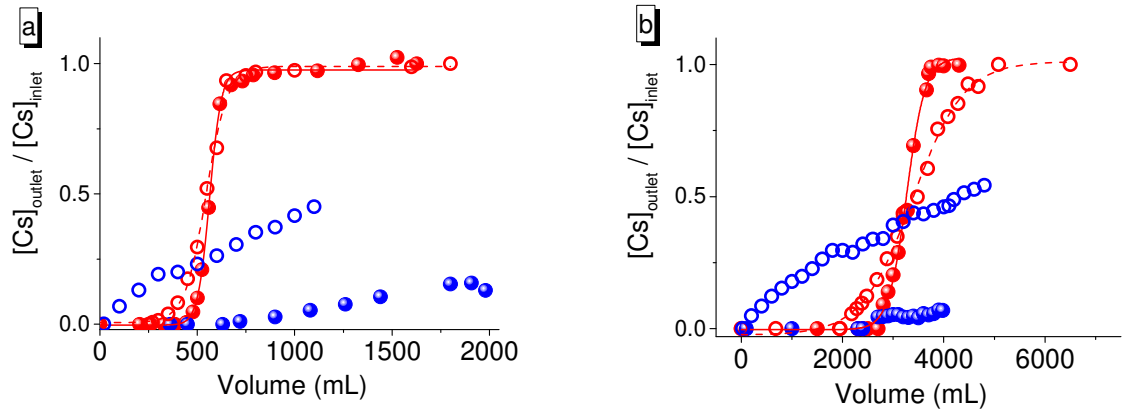

Fig. 9. Comparison of the breakthrough curves (($[Cs]_{outlet}/[Cs]_{inlet}$ vs. percolated volume) measured for Sorbmatech (red) and CST (blue) at (a) $[Cs]_{inlet}$ = 30mg·L^{-1} and (b) $[Cs]_{inlet}$ = 5 mg·L^{-1} and Darcy velocities of 5 m·h^{-1} (open circles) and 1 m·h^{-1} (full circles). Sorbmatech, mesoporous silica functionalized with potassium-copper hexacyanoferrate nanoparticles; CST, Nb-substituted Na crystalline silicotitanate.

4. Conclusions

The aim of this study was to highlight the key factors that determine the efficiency of a sorbent for the decontamination of trace elements in effluents. Most studies focus on the maximum sorption capacity but our comparison of three Cs sorbents shows that this parameter is potentially misleading for applications with low contaminant concentrations. Indeed, while chabazite has a high maximum sorption capacity for Cs, its distribution coefficient is low meaning that it has a low breakthrough volume in column processes. Decontaminating effluents with trace concentrations of Cs using chabazite in a continuous flow setup would therefore require prohibitively large volumes of the sorbent to be effective.

The two other sorbents studied here behave differently. CST has both a high maximum sorption capacity and a high distribution coefficient; Sorbmatech has a lower maximum sorption capacity but a similarly high distribution constant. Both are suitable for the removal of trace level Cs in batch mode. In a fixed bed column however, Sorbmatech shows near-ideal

breakthrough behavior with a sharp jump, even at high flow rates, due to fast Cs exchange kinetics, while the breakthrough curves measured for CST are featureless. The slower sorption kinetics of CST mean that Cs leakage occurs immediately at higher flow rates. Therefore, even though Sorbmatech has the lowest maximum Cs sorption capacity of the three materials considered here, its more favorable exchange kinetics and selectivity make it the most suitable for the removal by column treatment of trace-level Cs contamination. The next step consists into the transformation of the spent sorbent into a final waste form, as it is under progress by thermal treatment in case of Sorbmatech [40] [16]and in case of zeolithic materials [41-43]

Acknowledgments

This research was supported in part by the French government's "Programme d'Investissements d'Avenir" through the DEMETERRES Project (ANR-11-RSNR-005), with additional support from the CEA's RDAAD project and ORANO. The authors thank Anh-Hoang Le for the BET characterization of CST and chabazite, Joël Faure (LMAC laboratory, CEA Marcoule) for the ICP-AES analysis and Nicolas Massoni (LDMC, CEA Marcoule) for fruitful discussion and XRD experiments.

References

[1] X. Zhang, P. Gu, Y. Liu, Decontamination of radioactive wastewater: State of the art and challenges forward, Chemosphere, 215 (2019) 543-553. doi:https://doi.org/10.1016/j.chemosphere.2018.10.029

[2] M.A. Olatunji, M.U. Khandaker, H.N.M.E. Mahmud, Y.M. Amin, Influence of adsorption parameters on cesium uptake from aqueous solutions- a brief review, RSC Advances, 5 (2015) 71658-71683. doi:10.1039/c5ra10598f

[3] D. Alby, C. Charnay, M. Heran, B. Prelot, J. Zajac, Recent developments in nanostructured inorganic materials for sorption of cesium and strontium: Synthesis and shaping, sorption capacity, mechanisms, and selectivity—A review, Journal of Hazardous Materials, 344 (2018) 511-530. doi:https://doi.org/10.1016/j.jhazmat.2017.10.047
[4] C. Michel, Y. Barré, M. Ben Guiza, C. de Dieuleveult, L. De Windt, A. Grandjean, Breakthrough studies of the adsorption of Cs from freshwater using a mesoporous silica material containing ferrocyanide, Chemical Engineering Journal, 339 (2018) 288-295. doi:https://doi.org/10.1016/j.cej.2018.01.101
[5] S.M. DePaoli, D.T. Bostick, A.J. Lucero, Analysis of breakthrough profiles based on gamma-ray emission along loaded packed bed columns : comparative evaluation of ionsiv® IE-911 and chabazite zeolite for the removal of radiostrontium and cesium from groundwater., Separation Science and Technology, 36 (2001) 941-957. doi:10.1081/ss-100103630
[6] C. Mahendra, P.M. Sathya Sai, C. Anand Babu, K. Revathy, K.K. Rajan, Analysis and modeling of fixed bed sorption of cesium by AMP-PAN, Journal of Environmental Chemical Engineering, 3 (2015) 1546-1554. doi:https://doi.org/10.1016/j.jece.2015.05.002
[7] J.E. Miller, N.E. Brown, Development and Properties of Crystalline Silicotitanate (CST) Ion Echangers for radioactive waste applications, Sandia National Laboratory, Albuquerque (1997) 61
[8] A.J. Celestian, J.D. Kubicki, J. Hanson, A. Clearfield, J.B. Parise, The Mechanism Responsible for Extraordinary Cs Ion Selectivity in Crystalline Silicotitanate, Journal of the American Chemical Society, 130 (2008) 11689-11694. doi:10.1021/ja801134a
[9] S. Chitra, S. Viswanathan, S.V.S. Rao, P.K. Sinha, Uptake of cesium and strontium by crystalline silicotitanates from radioactive wastes, Journal of Radioanalytical and Nuclear Chemistry, 287 (2011) 955-960. doi:10.1007/s10967-010-0867-z
[10] X. Zhao, Q. Meng, G. Chen, Z. Wu, G. Sun, G. Yu, L. Sheng, H. Weng, M. Lin, An acid-resistant magnetic Nb-substituted crystalline silicotitanate for selective separation of strontium and/or cesium ions from aqueous solution, Chemical Engineering Journal, 352 (2018) 133-142. doi:https://doi.org/10.1016/j.cej.2018.06.175
[11] A. Clearfield, A. Tripathi, D. Medvedev, A.J. Celestian, J.B. Parise, In situ type study of hydrothermally prepared titanates and silicotitanates, Journal of Materials Science, 41 (2006) 1325-1333. doi:10.1007/s10853-006-7317-x
[12] V. Van Speybroeck, K. Hemelsoet, L. Joos, M. Waroquier, R.G. Bell, C.R.A. Catlow, Advances in theory and their application within the field of zeolite chemistry, Chemical Society Reviews, 44 (2015) 7044-7111. doi:10.1039/c5cs00029g
[13] M. Kong, Z. Liu, T. Vogt, Y. Lee, Chabazite structures with Li+, Na+, Ag+, K+, NH4+, Rb+ and Cs+ as extra-framework cations, Microporous and Mesoporous Materials, 221 (2016) 253-263. doi:https://doi.org/10.1016/j.micromeso.2015.09.031
[14] W. Baek, S. Ha, S. Hong, S. Kim, Y. Kim, Cation exchange of cesium and cation selectivity of natural zeolites: Chabazite, stilbite, and heulandite, Microporous and Mesoporous Materials, 264 (2018) 159-166. doi:https://doi.org/10.1016/j.micromeso.2018.01.025
[15] M. Calligaris, G. Nardin, L. Randaccio, P.C. Chiaramonti, Cation-site location in a natural chabazite, Acta Crystallographica Section B, 38 (1982) 602-605. doi:doi:10.1107/S0567740882003483
[16] C. Cabaud, Y. Barré, L. De Windt, S. Gill, E. Dooryhée, M.P. Moloney, N. Massoni, A. Grandjean, Removing Cs within a continuous flow set-up by an ionic exchanger material

transformable into a final waste form, Adsorption, 25 (2019) 765-771. doi:10.1007/s10450-019-00040-6
[17] C. Michel, Y. Barré, L. De Windt, C. de Dieuleveult, E. Brackx, A. Grandjean, Ion exchange and structural properties of a new cyanoferrate mesoporous silica material for Cs removal from natural saline waters, Journal of Environmental Chemical Engineering, 5 (2017) 810-817. doi:http://dx.doi.org/10.1016/j.jece.2016.12.033
[18] S. Ayrault, C. Loos-Neskovic, M. Fedoroff, E. Gamier, D.J. Jones, Compositions and structures of copper hexacyanoferrates(II) and (III): experimental results, Talanta, 42 (1995) 1581-1593
[19] D.O. Ojwang, J. Grins, D. Wardecki, M. Valvo, V. Renman, L. Haggstrom, T. Ericsson, T. Gustafsson, A. Mahmoud, R.P. Hermann, G. Svensson, Structure Characterization and Properties of K-Containing Copper Hexacyanoferrate, Inorganic Chemistry, 55 (2016) 5924-5934. doi:10.1021/acs.inorgchem.6b00227
[20] M.P. Moloney, C. Cabaud, N. Massoni, S. Stafford, Y.K. Gun'ko, M. Venkatesan, A. Grandjean, Searching for the nano effect in Cu-HCF (II) particles to improve Cs sorption efficiency: Highlighting the use of intrinsic magnetism, Colloids and Surfaces A: Physicochemical and Engineering Aspects, 582 (2019) 123758. doi:https://doi.org/10.1016/j.colsurfa.2019.123758
[21] S.N. Ghosh, Infrared spectra of the Prussian blue analogs, Journal of Inorganic and Nuclear Chemistry, 36 (1974) 2465-2466. doi:https://doi.org/10.1016/0022-1902(74)80454-9
[22] K. Venkatesan, V. Sukumaran, M. Antony, T. Srinivasan, Studies on the feasibility of using crystalline silicotitanates for the separation of cesium-137 from fast reactor high-level liquid waste, Journal of Radioanalytical and Nuclear Chemistry, 280 (2009) 129-136. doi:10.1007/s10967-008-7422-1
[23] J. Causse, A. Tokarev, J. Ravaux, M. Moloney, Y. Barré, A. Grandjean, Facile one-pot synthesis of copper hexacyanoferrate nanoparticle functionalised silica monoliths for the selective entrapment of 137Cs, Journal of Materials Chemistry A, 2 (2014) 9461. doi:10.1039/c4ta01266f
[24] G. Limousin, J.P. Gaudet, L. Charlet, S. Szenknect, V. Barthès, M. Krimissa, Sorption isotherms: A review on physical bases, modeling and measurement, Applied Geochemistry, 22 (2007) 249-275. doi:https://doi.org/10.1016/j.apgeochem.2006.09.010
[25] S.M. Robinson, W.D. Arnold, C.H. Byers, Mass-transfer mechanisms for zeolite ion exchange in wastewater treatment, AIChE Journal, 40 (1994) 2045-2054. doi:doi:10.1002/aic.690401214
[26] T. Vincent, C. Vincent, Y. Barré, Y. Guari, G. Le Saout, E. Guibal, Immobilization of metal hexacyanoferrates in chitin beads for cesium sorption: synthesis and characterization, Journal of Materials Chemistry A, 2 (2014) 10007. doi:10.1039/c4ta01128g
[27] S. Chitra, R. Sudha, S. Kalavathi, A.G.S. Mani, S.V.S. Rao, P.K. Sinha, Optimization of Nb-substitution and Cs+/Sr+2 ion exchange in crystalline silicotitanates (CST), Journal of Radioanalytical and Nuclear Chemistry, 295 (2013) 607-613. doi:10.1007/s10967-012-1812-0
[28] S.M. Depaoli, J.J. Perona, Model for Sr+Cs+Ca+Mg+Na ion-exchange uptake kinetics on chabazite, AIChE Journal, 42 (1996) 3434-3441. doi:doi:10.1002/aic.690421213
[29] C.F. Poole, A.D. Gunatilleka, R. Sethuraman, Contributions of theory to method development in solid-phase extraction, Journal of Chromatography A, 885 (2000) 17-39. doi:https://doi.org/10.1016/S0021-9673(00)00224-7

[30] K. Bielicka-Daszkiewicz, A. Voelkel, Theoretical and experimental methods of determination of the breakthrough volume of SPE sorbents, Talanta, 80 (2009) 614-621. doi:https://doi.org/10.1016/j.talanta.2009.07.037
[31] C.K. Rojas-Mayorga, A. Bonilla-Petriciolet, F.J. Sánchez-Ruiz, J. Moreno-Pérez, H.E. Reynel-Ávila, I.A. Aguayo-Villarreal, D.I. Mendoza-Castillo, Breakthrough curve modeling of liquid-phase adsorption of fluoride ions on aluminum-doped bone char using micro-columns: Effectiveness of data fitting approaches, Journal of Molecular Liquids, 208 (2015) 114-121. doi:https://doi.org/10.1016/j.molliq.2015.04.045
[32] S.C. Motshekga, S.S. Ray, Highly efficient inactivation of bacteria found in drinking water using chitosan-bentonite composites: Modelling and breakthrough curve analysis, Water Research, 111 (2017) 213-223. doi:https://doi.org/10.1016/j.watres.2017.01.003
[33] K. Yaghmaeian, G. Moussavi, A. Alahabadi, Removal of amoxicillin from contaminated water using NH4Cl-activated carbon: Continuous flow fixed-bed adsorption and catalytic ozonation regeneration, Chemical Engineering Journal, 236 (2014) 538-544. doi:https://doi.org/10.1016/j.cej.2013.08.118
[34] A. Galarneau, A. Sachse, B. Said, C.-H. Pelisson, P. Boscaro, N. Brun, L. Courtheoux, N. Olivi-Tran, B. Coasne, F. Fajula, Hierarchical porous silica monoliths: A novel class of microreactors for process intensification in catalysis and adsorption, Comptes Rendus Chimie, 19 (2016) 231-247. doi:https://doi.org/10.1016/j.crci.2015.05.017
[35] Y. Didi, B. Said, T. Cacciaguerra, K.L. Nguyen, V. Wernert, R. Denoyel, D. Cot, W. Sebai, M.-P. Belleville, J. Sanchez-Marcano, F. Fajula, A. Galarneau, Synthesis of binderless FAU-X (13X) monoliths with hierarchical porosity, Microporous and Mesoporous Materials, 281 (2019) 57-65. doi:https://doi.org/10.1016/j.micromeso.2019.03.003
[36] Y. Didi, B. Said, M. Micolle, T. Cacciaguerra, D. Cot, A. Geneste, F. Fajula, A. Galarneau, Nanocrystals FAU-X monoliths as highly efficient microreactors for cesium capture in continuous flow, Microporous and Mesoporous Materials, 285 (2019) 185-194. doi:https://doi.org/10.1016/j.micromeso.2019.05.012
[37] A. Sachse, A. Merceille, Y. Barré, A. Grandjean, F. Fajula, A. Galarneau, Macroporous LTA-monoliths for in-flow removal of radioactive strontium from aqueous effluents: Application to the case of Fukushima, Microporous and Mesoporous Materials, 164 (2012) 251-258. doi:https://doi.org/10.1016/j.micromeso.2012.07.019
[38] B. Said, A. Grandjean, Y. Barre, F. Tancret, F. Fajula, A. Galarneau, LTA zeolite monoliths with hierarchical trimodal porosity as highly efficient microreactors for strontium capture in continuous flow, Microporous and Mesoporous Materials, 232 (2016) 39-52. doi:http://dx.doi.org/10.1016/j.micromeso.2016.05.036
[39] Z.Z. Chowdhury, S.M. Zain, A.K. Rashid, R.F. Rafique, K. Khalid, Breakthrough Curve Analysis for Column Dynamics Sorption of Mn(II) Ions from Wastewater by Using Mangostana garcinia Peel-Based Granular-Activated Carbon, Journal of Chemistry, http://dx.doi.org/10.1155/2013/959761. Article ID 959761. (2013)
[40] N. Massoni, R.J. Koch, A. Hertz, L. Campayo, M.P. Moloney, S.T. Misture, A. Grandjean, Structural effects of calcination on Cs-exchanged copper hexacyanoferrate (Cs,K)2CuFe(CN)6 loaded on mesoporous silica particles, Journal of Nuclear Materials, 528 (2020) 151887. doi:https://doi.org/10.1016/j.jnucmat.2019.151887
[41] P. Bosch, D. Caputo, B. Liguori, C. Colella, Safe trapping of Cs in heat-treated zeolite matrices, Journal of Nuclear Materials, 324 (2004) 183-188. doi:10.1016/j.jnucmat.2003.10.001

[42] B. Liguori, D. Caputo, F. Iucolano, P. Aprea, B. de Gennaro, Entrapping of Cs and Sr in heat-treated zeolite matrices, Journal of Nuclear Materials, 435 (2013) 196-201. doi:https://doi.org/10.1016/j.jnucmat.2012.12.043
[43] A. Brundu, G. Cerri, Thermal transformation of Cs-clinoptilolite to CsAlSi5O12, Microporous and Mesoporous Materials, 208 (2015) 44-49. doi:10.1016/j.micromeso.2015.01.029